The Astrophysical Journal, 1009:157 (10pp), 2026 October 1 https://doi.org/10.3847/1538-4357/ae99e6
© 2026. The Author(s). Published by the American Astronomical Society.
OPEN ACCESS

SN 2023gfo: A Peculiar Type IIP Supernova with High Luminosity and Normal Plateau Duration

Riko Namba[1,2], Masayuki Yamanaka[3], Keiichi Maeda[4], Avinash Singh[5], Kenta Taguchi[4,6], Takahiro Nagayama[1], Miho Kawabata[6], Koji S. Kawabata[7], Tatsuya Nakaoka[7], Devendra Sahu[8], Anjasha Gangopadhyay[5], and G. C. Anupama[8]

[1] Graduate School of Science and Engineering, Kagoshima University, 1-21-35 Korimoto, Kagoshima, Kagoshima 890-0065, Japan
[2] Department of Physics and Astronomy, Faculty of Science, Kagoshima University, 1-21-35 Korimoto, Kagoshima, Kagoshima 890-0065, Japan
[3] Amanogawa Galaxy Astronomy Research Center (AGARC), Graduate School of Science and Engineering, Kagoshima University, 1-21-35 Korimoto, Kagoshima, Kagoshima 890-0065, Japan
[4] Department of Astronomy, Kyoto University, Kitashirakawa-Oiwake-cho, Sakyo-ku, Kyoto 606-8502, Japan
[5] Oskar Klein Centre, Department of Astronomy, Stockholm University, AlbaNova, SE-106 91 Stockholm, Sweden
[6] Okayama Observatory, Kyoto University, 3037-5 Honjo, Kamogatacho, Asakuchi, Okayama 719-0232, Japan
[7] Hiroshima Astrophysical Science Center, Hiroshima University, 1-3-1 Kagamiyama, Higashi-Hiroshima, Hiroshima 739-8526, Japan
[8] Indian Institute of Astrophysics, Koramangala 2nd Block, Bangalore 560034, India
Received 2026 March 26; revised 2026 July 12; accepted 2026 August 13; published 2026 September 25

Abstract

We present near-infrared (NIR) and optical observations of the highly reddened Type IIP supernova (SN) 2023gfo in the nearby galaxy NGC 4995 ($d = 26.4 \pm 3.2$ Mpc), which reached a high peak luminosity of $M_V = -18.6$ mag. The SN was initially detected as a faint red event, with $B - V = 0.8$ mag at the beginning of the plateau phase. By comparison with the template, we estimate a total extinction of $A_V = 2.1$ mag. After correcting for this extinction, we derive a peak quasi-bolometric luminosity of $(5.9 \pm 1.5) \times 10^{42}$ erg s^{-1}, placing this event among the most luminous SNe IIP, while its plateau duration remains within the normal range. The early-phase optical spectrum exhibits a P-Cygni profile of Hα, with a broad absorption of $V = 13{,}800$ km s^{-1}, which is among the highest observed for SNe IIP at comparable epochs. The high luminosity and the normal plateau duration suggest that this event represents an outlier. Applying an analytical model, we infer an unusually large progenitor radius. This may indicate that the progenitor experienced an extreme energy injection from the core to the envelope shortly before explosion, resulting in a substantially inflated radius. While ejecta–circumstellar matter (CSM) interaction could in principle account for the high luminosity, we find no observational evidence supporting strong interaction.

Unified Astronomy Thesaurus concepts: Type II supernovae (1731); Core-collapse supernovae (304)

1. Introduction

Massive stars ($M_{\rm ZAMS} > 8$–$10\,M_\odot$; A. Heger et al. 2003) reach the end of their evolutionary stage and subsequently undergo core-collapse supernovae (CCSNe), i.e., terminal explosions of massive stars. Those events characterized by the presence of hydrogen lines in their optical spectra are classified as Type II SNe (SNe II; R. Minkowski 1941; A. V. Filippenko 1997). Type IIP SNe constitute the most common subclass of CCSNe, accounting for approximately half of all observed events (W. Li et al. 2011). They are characterized by an extended plateau phase in their optical light curves, lasting for several months. This plateau is generally attributed to the recombination of hydrogen in the massive envelope retained by the progenitor star at the time of explosion. Despite the growing number of observations, the connection between progenitor properties and the observable characteristics of SNe IIP remains poorly constrained and continues to be actively debated.

Observational diversity is seen in several observed properties among SNe IIP. Their absolute peak magnitudes in the V band show a wide distribution, typically ranging from approximately −15 to −18 mag (J. P. Anderson et al. 2014). This diversity extends to their temporal evolution; previous studies have established several key statistical correlations linking their photometric features. Furthermore, a proportional relationship between luminosity and expansion velocity has also been found (M. Hamuy 2003), emphasizing the intrinsic links between explosion energy, the amount of radioactive nickel synthesized, and the resulting photometric diversity of SNe IIP.

Recently, highly ionized emission lines with a blue continuum were detected for some Type IIP SNe during their early phases (D. Khazov et al. 2016; O. Yaron et al. 2017). The high ionization temperature indicates that the surrounding gas is ionized by the strong radiation field emanating from the central SN. This "flash feature" infers that a progenitor is surrounded by a dense and compact circumstellar matter (CSM) located at $\sim 10^{14}$–10^{15} cm, frequently referred to as the "confined CSM". Given the typical ejecta velocity, the ejecta quickly sweeps up the confined CSM. In such a situation, the interaction power causes a faster rise and bumpy structure in the early-phase light curve (T. J. Moriya & A. Singh 2024).

One possible scenario of confined CSM is enhanced mass loss driven by increased stellar activity in the final stages of stellar evolution. However, the observational consequences of such late-stage energy deposition are not yet fully understood. In some cases, it could lead to a substantial radius expansion rather than the formation of the confined CSM, which is predicted to result in a peculiar SN IIP with a high luminosity and long plateau as compared to canonical SNe IIP (R. Ouchi & K. Maeda 2019).

Original content from this work may be used under the terms of the Creative Commons Attribution 4.0 licence. Any further distribution of this work must maintain attribution to the author(s) and the title of the work, journal citation and DOI.

R. Ouchi & K. Maeda (2021) showed that the observational properties of the peculiar SN IIP 2009kf, which has these properties (M. T. Botticella et al. 2010), could be explained within this scenario and derived a progenitor radius significantly larger than those of typical Type IIP SNe.

In this paper, we present optical and NIR observations of SN 2023gfo, a high-luminosity Type IIP SN. Section 2 details the telescopes and instruments used for the observations. Section 3 provides a detailed description of the extinction correction applied to the data. Then, we present the results, including the light curves, spectral data, and the bolometric light curve derived from our observations, comparing them with those of Type IIP SNe previously studied. In Section 4, we discuss the physical parameters of SN 2023gfo, where we find that the progenitor radius is larger than those of typical Type IIP SNe; a similar situation is found in SN 2009kf, and we suggest that the peculiar nature of SN 2023gfo could be explained by an inflated progenitor star caused by the final stellar activity. Section 5 summarizes our conclusions.

2. Observations and Data Reduction

SN 2023gfo was discovered at 16.2 mag by the Asteroid Terrestrial Impact Last Alert System (ATLAS; J. L. Tonry et al. 2018; K. W. Smith et al. 2020) on 2023 April 20 (UT) (MJD 60054.2) (J. Tonry et al. 2023). Prior to discovery, this object was detected at 19.2 mag on MJD 60051.2, while the last nondetection was reported at MJD 60050.0 with a limiting magnitude of 19.5 mag (J. Tonry et al. 2023). These observations indicate a rapid rise shortly after the explosion. Throughout this paper, we adopt an explosion epoch of MJD 60050.6 ($t = 0$). Spectroscopic observations subsequently classified SN 2023gfo as a Type IIP SN and revealed significant reddening along the line of sight (M. Fulton et al. 2023). Y. Yang et al. (2023) independently classified SN 2023gfo and adopted a host-galaxy redshift of $z = 0.00594$, corresponding to a recession velocity of approximately 1780 km s^{-1}. The redshift-independent distance of the host galaxy NGC 4995, primarily obtained using the Tully–Fisher (TF) method from the NASA/IPAC Extragalactic Database (NED), is 26.4 ± 3.2 Mpc. The corresponding distance modulus is 32.06 ± 0.42 mag (C. M. Springob et al. 2009; I. D. Karachentsev & O. G. Nasonova 2013; J. G. Sorce et al. 2014; R. B. Tully et al. 2013, 2016). Our adopted TF distance is consistent with the Hubble-flow (HF) distance provided by NED. According to NED, the HF distance corrected for the Virgo Cluster, the Great Attractor (GA), and the Shapley Supercluster is $m - M = 32.35 \pm 0.15$ mag. The agreement between these two independent distance indicators reinforces the reliability of our distance scale. We adopted these values throughout this paper.

Optical photometric observations in the *BVRI* bands were conducted using HOWPol (K. S. Kawabata et al. 2008) mounted on the 1.5 m Kanata Telescope located at Higashi-Hiroshima Observatory. Additional optical photometry in the *g*, *r*, *i*, and *z* bands was obtained with the GROWTH-India Telescope (GIT; R. Kumar et al. 2023) at the Indian Astronomical Observatory (IAO) in Hanle. We monitored SN 2023gfo in the NIR band using the kSIRIUS, which is the simultaneous NIR JHK_s-band imager (T. Nagayama & H. Nakaya 2024) attached to the Cassegrain focus of the Kagoshima 1.0 m Telescope at the Iriki Observatory.

All imaging data were reduced following standard procedures using the Image Reduction and Analysis Facility (IRAF; D. Tody 1986). The photometric magnitudes were obtained through point-spread-function photometry using standard IRAF tasks such as DAOPHOT (P. B. Stetson 1987). For the optical observations, the photometric calibration was performed using secondary stars from the Pan-STARRS catalog (H. A. Flewelling et al. 2020). For the NIR observations, the calibration was performed using the Two Micron All-Sky Survey catalog (2MASS; M. F. Skrutskie et al. 2006).

Optical spectroscopic observations were conducted over three nights using KOOLS-IFU (K. Matsubayashi et al. 2025) on the 3.8 m Seimei Telescope at the Okayama Observatory (M. Kurita et al. 2020). The data reduction was performed following standard procedures using IRAF (D. Tody 1986, 1993). Standard corrections for atmospheric extinction and telluric absorption were applied. IRAF is distributed by the National Optical Astronomy Observatory, which is operated by the Association of Universities for Research in Astronomy (AURA) under a cooperative agreement with the National Science Foundation.[9] The wavelength scale was corrected for the host-galaxy recession velocity corresponding to a redshift of $z = 0.00594$.

3. Results

3.1. Optical and Infrared Light Curves

Photometric monitoring of SN 2023gfo began at $t = 6$ days (see Figure 1). The *V*-band light curve showed a slight rise from 13.6 mag at $t = 5.2$ days to a peak magnitude of 13.5 mag at $t = 10.0$ days, followed by a subsequent decline (see Figure 1). In the NIR, the *J*-band light curve reached its maximum at approximately $t = 23$ days. The maximum date was reached later at longer wavelengths.

Figure 2 compares the *c*-band light curve of SN 2023gfo with the *V*-band light curves of the Carnegie Supernova Project (CSP) sample (J. P. Anderson et al. 2014), each normalized by its peak magnitude. It is within the distribution of the light curves of the CSP sample. The comparison between the ATLAS *c*-band and the literature *V*-band samples is justified because the *c*-band wavelength range encompasses the standard *V* band (J. L. Tonry et al. 2018), and the *c*-band light-curve distribution of SNe IIP is very similar to that of the *V* band (K. Ertini et al. 2026). Following the methodology of J. P. Anderson et al. (2014), we derived the plateau duration using the *c*-band light curve, finding a length of 108 ± 8 days. Therefore, in this study, we adopt a plateau duration of ∼108 days.

3.2. Extinction

SN 2023gfo exhibits significant reddening, requiring a correction for extinction. As an initial estimate, we measured the equivalent width (EW) of the Na I D absorption lines at the host-galaxy redshift ($z = 0.00594$), which yielded a value of ∼2.4 Å, indicative of substantial extinction (D. Poznanski et al. 2012). However, at such large EW values, the empirical relation proposed by D. Poznanski et al. (2012) becomes unreliable.

[9] Image Reduction and Analysis Facility (IRAF) was originally distributed by the National Optical Astronomy Observatory (NOAO), which was operated by the Association of Universities for Research in Astronomy (AURA) under a cooperative agreement with the National Science Foundation. IRAF is currently maintained by NSF NOIRLab. See https://iraf.noirlab.edu.

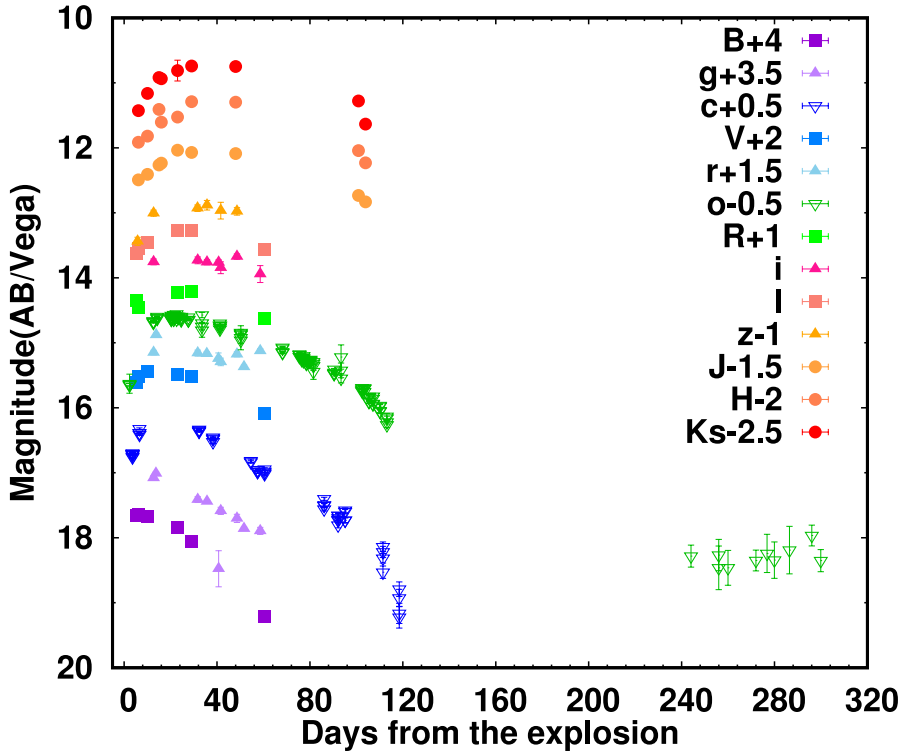


Figure 1. The optical and NIR light curve of SN 2023gfo. Photometric data are color-coded and plotted with various symbols: ATLAS *c* and *o* bands (squares), GIT *g*, *r*, *i*, and *z* bands (triangles), HOWPol *B*, *V*, *R*, and *I* bands (diamonds), and kSIRIUS *J*, *H*, and K_s bands (circles). The *B*, *V*, *R*, *I*, *J*, *H*, and K_s-band magnitudes are in the Vega system, and *c*, *o*, *g*, *r*, *i*, and *z*-band ones in the AB system. Each magnitude is artificially shifted to distinguish the light curves.

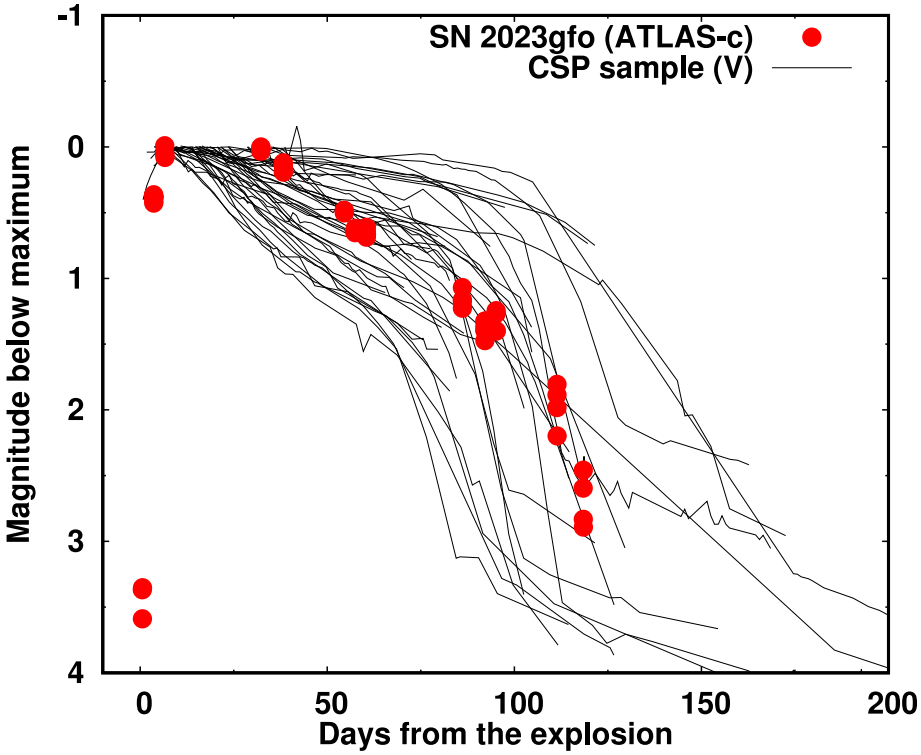


Figure 2. The ATLAS *c*-band and HOWPol *V*-band light curve of SN 2023gfo compared with the *V*-band ones of Type IIP SNe in the CSP sample (J. P. Anderson et al. 2014), normalized to the peak magnitude (set to zero).

We therefore applied another method to determine the extinction, primarily through a comparison of the observed color evolution with those of template Type IIP SNe. The optical spectrum obtained at $t = 11$ days shows typical absorption features of a normal Type IIP SN (see Section 3.6). The characteristic light-curve evolution is also consistent with typical SNe IIP (see Figure 2). These properties suggest that the plateau phase is shaped by hydrogen recombination. In this scenario, the

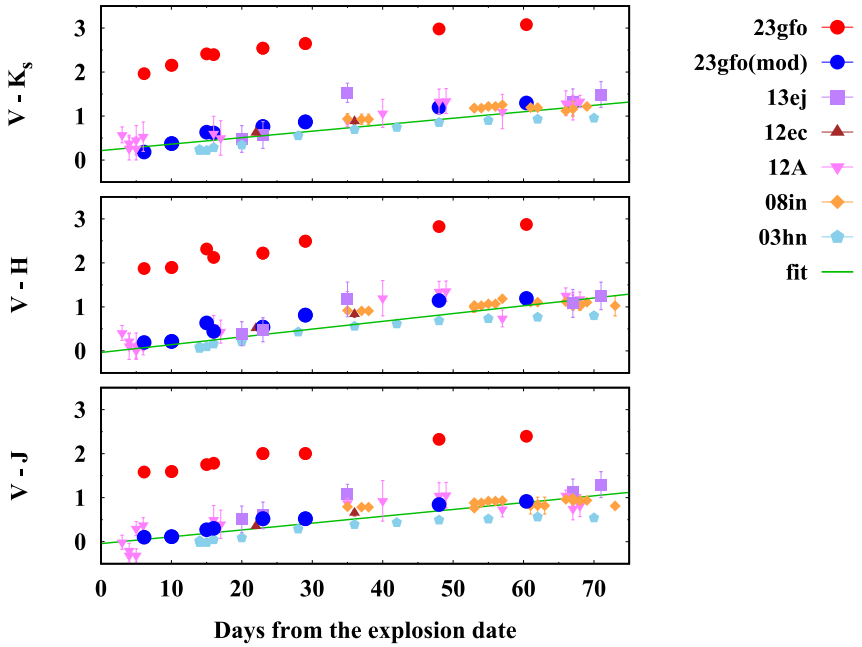


Figure 3. The V-JHK_s color evolution of SN 2023gfo compared with those of other SNe 2003hn (K. Krisciunas et al. 2009), 2008in (R. Roy et al. 2011), 2012A (L. Tomasella et al. 2013), 2012ec (C. Barbarino et al. 2015), and 2013ej (F. Huang et al. 2015). Blue points represent SN 2023gfo before the extinction correction, while red points show the extinction-corrected SN 2023gfo with $A_V = 2.1$ mag. The green solid line represents a linear function fit to combined data of comparative SNe.

photospheric temperatures of SNe IIP are expected to be similar, leading to relatively uniform intrinsic colors (L. Martinez et al. 2022). Based on this assumption, we applied methods for correcting extinction using color evolution (Figure 3).

We first estimated the V-band extinction using the $B - V$ color at 30 days after the explosion. Following the prescription of T. de Jaeger et al. (2018), this method yielded $E(B - V) = 0.52 \pm 0.19$ mag (see also Y. Yang et al. 2023), corresponding to $A_V = 1.6 \pm 0.6$ mag assuming $R_V = 3.1$ (J. A. Cardelli et al. 1989), although with a relatively large uncertainty.

To obtain a more robust estimate, we constructed color curves by combining V and JHK_s-band photometry. For the intrinsic $V - JHK_s$ colors, we adopted template color derived from linear fits to merged data of SNe 2003hn (K. Krisciunas et al. 2009), 2008in (R. Roy et al. 2011), 2012ec (C. Barbarino et al. 2015), 2012A (L. Tomasella et al. 2013), and 2013ej (F. Huang et al. 2015), using data until $t = 70$ days. Using these templates, we derived color excesses for SN 2023gfo of $E(V - J) = 1.6 \pm 0.1$ mag, $E(V - H) = 1.9 \pm 0.1$ mag, and $E(V - K_s) = 1.9 \pm 0.1$ mag. Adopting a Galactic extinction law ($R_V = 3.1$), these values correspond to an extinction of $A_V = 2.1 \pm 0.1$ mag. It is important to note that the NIR magnitudes are significantly less sensitive to the choice of R_V compared to the optical V band. For instance, even with $A_V = 2.1$ mag, the extinction in the K_s band is as small as $A_{K_s} = 0.17$ mag. This low sensitivity to R_V uncertainties ensures a more robust derivation of the intrinsic luminosity. Given the smaller uncertainty associated with the $V - JHK_s$ estimate, we adopt $A_V = 2.1$ mag to correct all observational data presented in this study. As independent support for this extinction value, the A_V-corrected spectra exhibit an Hα/Hβ flux ratio that is consistent with the intrinsic Balmer decrement expected for Case B recombination (D. E. Osterbrock & G. J. Ferland 2006). This agreement confirms the validity of our adopted $A_V = 2.1$ mag.

3.3. Absolute Magnitude

We derived the absolute magnitudes of SN 2023gfo after correcting for extinction and distance modulus. For comparison, we compiled photometric data of SNe 1999em (A. Elmhamdi et al. 2003), 2003hn (K. Krisciunas et al. 2009), 2004et (K. Maguire et al. 2010), 2005cs (A. Pastorello et al. 2009), 2008in (R. Roy et al. 2011), 2012A (L. Tomasella et al. 2013), 2012ec (C. Barbarino et al. 2015), 2013ej (F. Huang et al. 2015), and 2023ixf (M. Yamanaka et al. 2023; A. Singh et al. 2024). The resulting absolute-magnitude light curves are shown in Figure 4. In the NIR bands, SN 2023gfo is significantly brighter than the comparison Type IIP SNe. In particular, its peak absolute magnitude reaches $M_{K_s} = -19.5 \pm 0.4$ mag. Consistently, SN 2023gfo is also brighter in the J and H bands than all comparison objects. In the optical, we further compared the V-band absolute magnitude of SN 2023gfo with the sample presented by J. P. Anderson et al. (2014). SN 2023gfo reaches a peak absolute magnitude of $M_V = -18.6 \pm 0.4$ mag, placing it among the most luminous Type IIP SNe observed to date. For reference, even the most luminous events in the J. P. Anderson et al. (2014) sample reach peak magnitudes of $M_V = -18.3 \pm 0.4$ mag. These comparisons demonstrate that SN 2023gfo is an exceptionally luminous Type IIP SN.

We examined the plateau duration and the peak absolute magnitude of SN 2023gfo relative to the distribution of V-band light curves in the CSP sample (see Figure 5). For comparison, the values for SN 2009kf are also shown. We find that the plateau duration of SN 2023gfo and SN 2009kf is close to the mode of the CSP distribution, indicating plateau durations that are typical of Type IIP SNe. In contrast, their absolute magnitudes are located at the extreme luminous end of the distribution. In summary, while SN 2023gfo exhibits a plateau duration and light-curve morphology consistent with those of normal Type IIP SNe, its peak luminosity is exceptionally high compared to the bulk of the population.

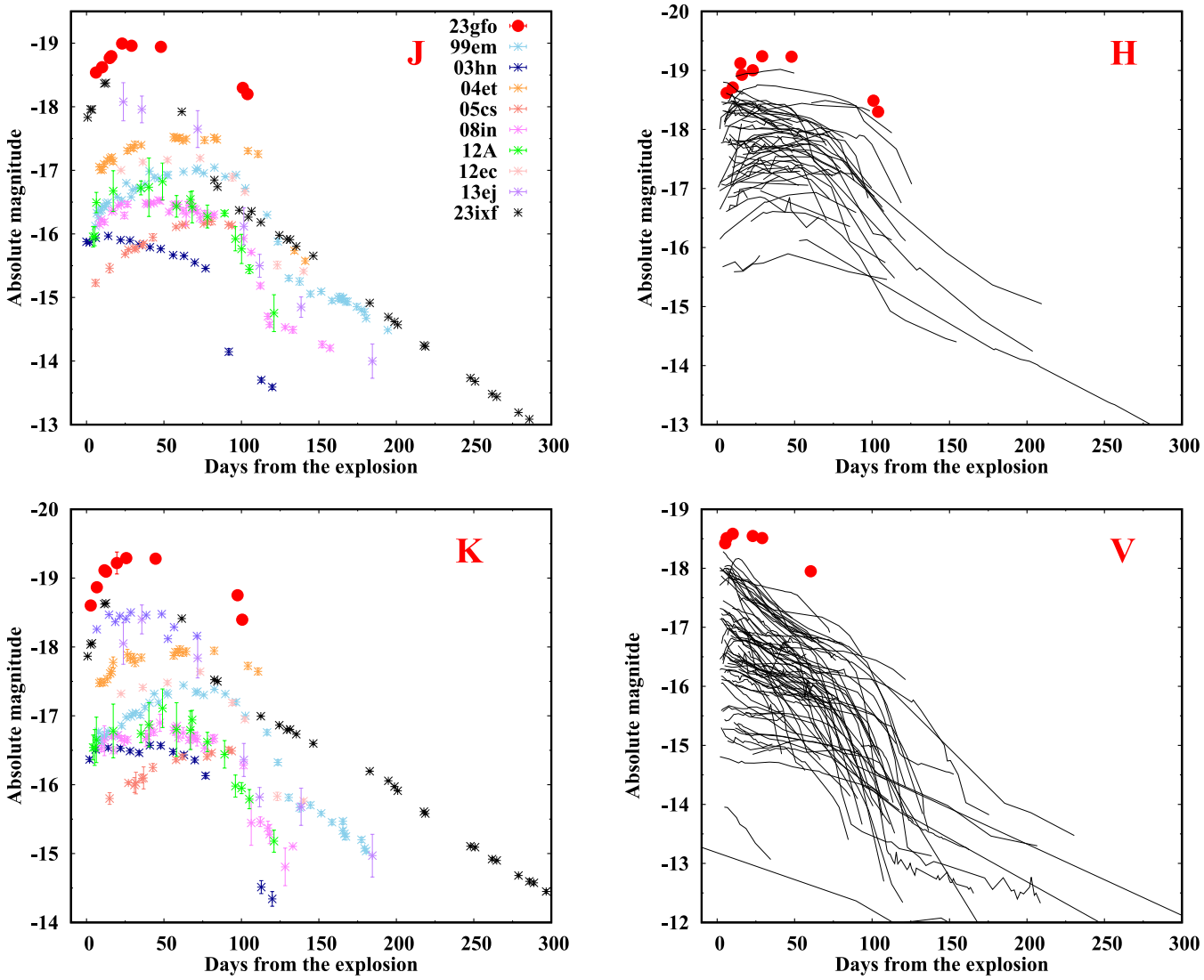


Figure 4. The J (top left), H (top right), K_s (bottom left), and V-band (bottom right) absolute magnitude light curves of SN 2023gfo. The J and K_s-band light curves are compared with those of SNe 1999em (A. Elmhamdi et al. 2003), 2003hn (K. Krisciunas et al. 2009), 2004et (K. Maguire et al. 2010), 2005cs (A. Pastorello et al. 2009), 2008in (R. Roy et al. 2011), 2012A (L. Tomasella et al. 2013), 2012ec (C. Barbarino et al. 2015), 2013ej (F. Huang et al. 2015), and 2023ixf (M. Yamanaka et al. 2023; A. Singh et al. 2024). For the V and H bands, the samples from L. Martinez et al. (2022) are shown for comparison. The red points in each graph denote SN 2023gfo. The absolute magnitudes of SN 2023gfo were corrected using the extinction values obtained in this study ($A_V = 2.1$ mag, $A_J = 0.51$ mag, $A_H = 0.3$ mag, and $A_{K_s} = 0.17$ mag), while those of other objects were corrected using the extinction values and distances from their respective literature.

3.4. Bolometric Light Curve

Using optical and NIR photometry, we constructed the bolometric light curve of SN 2023gfo based on the extinction-corrected magnitudes. The observed magnitudes were converted to flux densities at the effective wavelengths of each filter (M. Fukugita et al. 1996), and the resulting spectral energy distribution was integrated over wavelength to obtain the bolometric luminosity. In this study, the bolometric luminosity is defined as a pseudo-bolometric luminosity derived from the $BVRIJHK_s$ bands. For consistency, we derived pseudo-bolometric light curves for other Type IIP SNe using the same filter set and methodology. Figure 6 compares the $BVRIJHK_s$ pseudo-bolometric light curve of SN 2023gfo with those of other Type IIP SNe. SN 2023gfo reaches a maximum bolometric luminosity of $(5.9 \pm 1.5) \times 10^{42}$ erg s^{-1} at $t = 23.6$ days. This peak luminosity is significantly higher than those of the comparison objects at similar phases.

3.5. Optical Spectroscopy

Optical spectroscopic observations were obtained at $t = 4$, 5, and 11 days after the estimated explosion date (Figure 7). In the following, we focus on the spectrum at $t = 11$ days, which allows detailed analysis of spectral features thanks to its high signal-to-noise ratio. The $t = 11$ days spectrum of SN 2023gfo is compared with those of SNe 2007od (C. Inserra et al. 2011), 2004et (D. K. Sahu et al. 2006), and 2013ej (S. Valenti et al. 2014) at similar phases. The spectrum exhibits a prominent P-Cygni profile in Hα, with an expansion velocity of approximately 13,800 km s^{-1}. Broad absorption features of Hβ and He Iλ5876 are also clearly detected. The inferred expansion velocity is among the highest reported for Type IIP SNe at comparable epochs.

The spectra show narrow emission lines of Hα, [N II], and [S II], which originate from the underlying H II region within the host galaxy. We measured the ratios of these emission line strengths. Based on the method described in

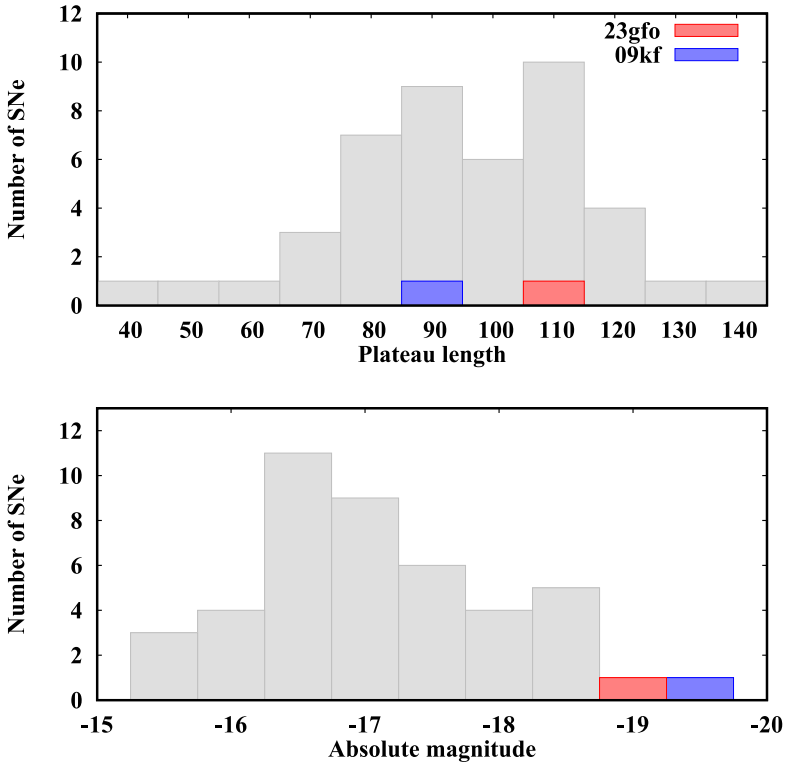


Figure 5. Top: distribution of the plateau length, as defined by J. P. Anderson et al. (2014), for the CSP Type II SN sample. The positions of SN 2023gfo and SN 2009kf are indicated in red and blue, respectively. Bottom: distribution of the peak absolute magnitudes in the *V* band for the same sample, with SN 2023gfo and SN 2009kf highlighted.

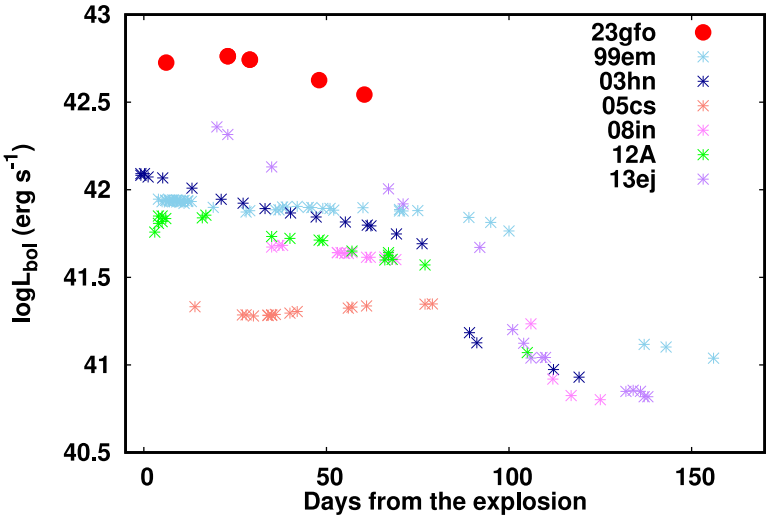


Figure 6. The bolometric light curve of SN 2023gfo compared with those of SNe 1999em (A. Elmhamdi et al. 2003), 2003hn (K. Krisciunas et al. 2009), 2005cs (A. Pastorello et al. 2009), 2008in (R. Roy et al. 2011), 2012A (L. Tomasella et al. 2013), and 2013ej (F. Huang et al. 2015). The red point represents SN 2023gfo. The horizontal axis shows days since explosion, and the vertical axis shows the logarithm of the bolometric luminosity.

M. Pettini & B. E. J. Pagel (2004), we estimated the metallicity at the SN site to be 8.7, and found it to be consistent with the average value for Type II SNe (J. P. Anderson et al. 2010).

4. Discussion

Section 3 highlighted the key properties of SN 2023gfo, including the plateau duration, expansion velocity, and bolometric luminosity. SN 2023gfo is characterized by a high luminosity ($M_V = -18.6$ mag) and a high expansion velocity ($v_{H\alpha} = 13{,}800\,\mathrm{km\,s^{-1}}$), despite its normal plateau length ($t_p = 108$ days). This combination places SN 2023gfo as an outlier relative to the distribution of Type IIP SNe.

Although SN 2023gfo lies at the luminous end of the Type IIP population, R. Ouchi & K. Maeda (2019) demonstrated through radiation-hydrodynamic calculations that the analytic scaling relations of D. V. Popov (1993) and D. Kasen & S. E. Woosley (2009) successfully reproduce the plateau luminosities and durations of Type IIP SN models with expanded envelopes. This result supports the applicability of

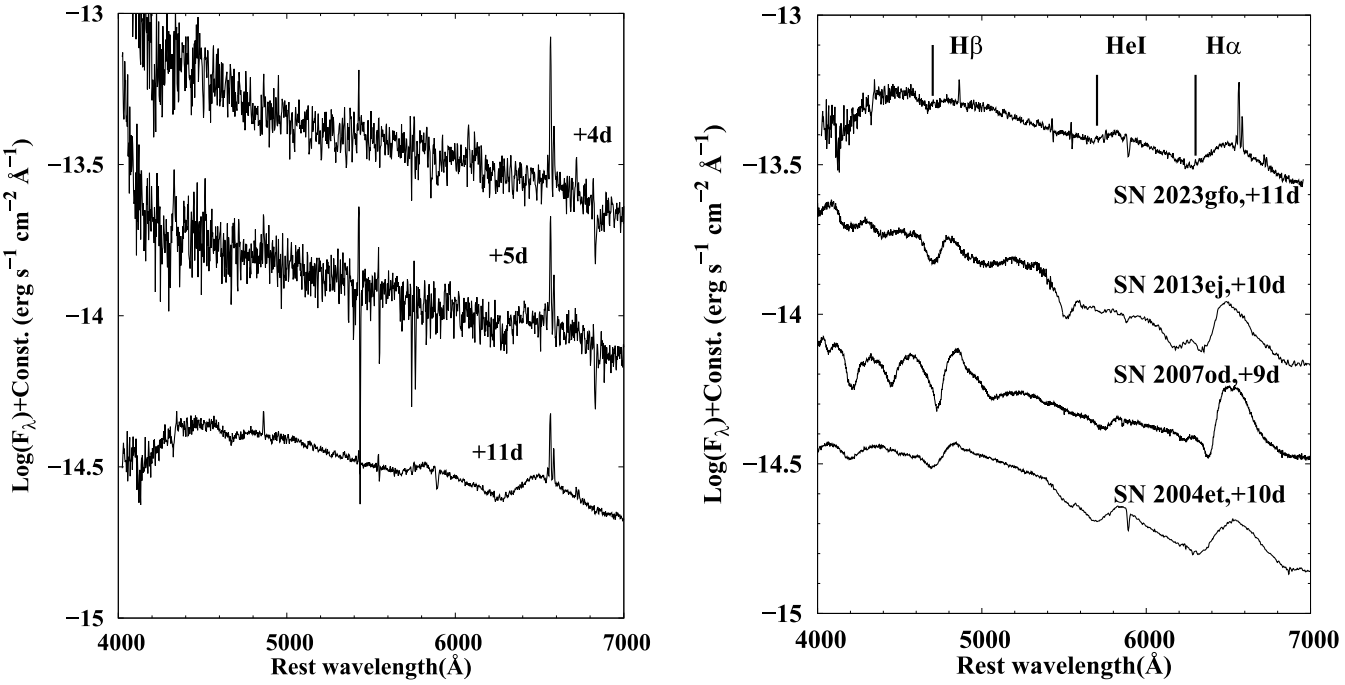


Figure 7. (Left) Optical spectra of SN 2023gfo obtained at $t = 4$, 5, and 11 days, displayed from top to bottom, respectively. The flux has been corrected for the total line-of-sight extinction, dominated by the host-galaxy component, using $A_V = 2.1$ mag. The spectra are shown in the rest frame of the host galaxy, determined from the narrow host-galaxy emission lines. (Right) Optical spectrum of SN 2023gfo at $t = 11$ days, compared with spectra of Type IIP SNe 2007od (C. Inserra et al. 2011), 2004et (D. K. Sahu et al. 2006), and 2013ej (S. Valenti et al. 2014) as similar phases.

these scaling relations even in the high-luminosity regime represented by SN 2023gfo. We therefore estimated the physical properties of SN 2023gfo using the analytic scaling relations of D. V. Popov (1993) and D. Kasen & S. E. Woosley (2009). As a primary reference object, we adopted SN 2009kf, whose observational properties closely resemble those of SN 2023gfo. SN 2009kf exhibited an unusually high luminosity and a large expansion velocity while maintaining a plateau duration comparable to those of normal Type IIP SNe (M. T. Botticella et al. 2010). Furthermore, R. Ouchi & K. Maeda (2021) derived its physical properties through radiation-hydrodynamic modeling and reported a progenitor radius exceeding 6000 $R_\odot$.

Using SN 2009kf as the primary reference object, we estimated the explosion and progenitor properties of SN 2023gfo using the analytic scaling relations of D. V. Popov (1993) and D. Kasen & S. E. Woosley (2009):

$$L_{\rm SN} \propto E_{\rm k}^{5/6} M_{\rm ej}^{-1/2} R_0^{2/3} \kappa^{-1/3} T_{\rm I}^{4/3}, \quad (1)$$

$$t_{\rm SN} \propto E_{\rm k}^{-1/6} M_{\rm ej}^{1/2} R_0^{1/6} \kappa^{1/6} T_{\rm I}^{-2/3}, \quad (2)$$

$$v_{\rm SN} \approx \left(\frac{2E_{\rm k}}{M_{\rm ej}}\right)^{1/2}, \quad (3)$$

where $L_{\rm SN}$ and $t_{\rm SN}$ are the luminosity and duration of the plateau phase. $v_{\rm SN}$ denotes the ejecta velocity. $E_{\rm k}$, $M_{\rm ej}$, and R_0 denote the explosion energy, ejecta mass, and pre-SN progenitor radius, respectively. κ and $T_{\rm I}$ are the opacity and ionization temperature, respectively, which can be taken to be universal among different objects.

The Hα absorption minimum of SN 2023gfo was measured to be 13,800 km s^{-1} at $t = 11$ days. Since spectra around the middle of the plateau phase were not available, we estimated the expansion velocity at $t = 60$ days by fitting the velocity evolution of SN 2017eaw using an exponential function and scaling it to match the observed velocity of SN 2023gfo. The resulting velocity at $t = 60$ days was approximately 7000 km s^{-1} and was adopted for the scaling analysis (see Table 1).

Table 1
Observed Properties Adopted for the Scaling Analysis

SN	v_{60} (km s^{-1})	$t_{\rm p}$ (days)	$L_{\rm bol}(60)$ (erg s^{-1})
SN 2009kf	9000	~90	6.3×10^{42}
SN 2023gfo	7000	108	3.5×10^{42}

Table 2
Physical Properties of SN 2009kf and the Scaled Values for SN 2023gfo

SN	$E_{\rm k}$ (foe)	$M_{\rm ej}$ ($M_\odot$)	R_0 ($R_\odot$)
SN 2009kf	2.8	11	6000
SN 2023gfo	3.0	19.3	3500

For the comparison objects, velocities measured at similar phases were adopted. The bolometric luminosity was $(3.5 \pm 1.5) \times 10^{42}$ erg s^{-1} at $t = 60$ days for SN 2023gfo. The luminosities at similar phases were used for comparison with SNe, ensuring a consistent comparison.

The inferred progenitor radius is substantially larger than those typically expected for generally red supergiant progenitors of Type IIP SNe. However, a similarly large progenitor radius was also derived for SN 2009kf by R. Ouchi & K. Maeda (2021) (see Table 2). Moreover, the explosion energies inferred for SN 2023gfo and SN 2009kf are comparable, while the ejecta mass estimated for SN 2023gfo

Table 3
Physical Parameters Adopted for the Reference SNe and the Corresponding Parameters Derived for SN 2023gfo

Reference SN	Reference SN			Derived for SN 2023gfo			
	E_k (foe)	M_{ej} ($M_\odot$)	R_0 ($R_\odot$)	Reference	E_k (foe)	M_{ej} ($M_\odot$)	R_0 ($R_\odot$)
SN 2009kf	2.8	11	6000	(1)	3.0	19	3500
SN 1999em	1.25	19	800	(2)	1.8	15	3900
SN 2012A	0.48	12.5	259	(3)	0.6	11	3600
SN 2012aw	1.5	20	430	(4)	2.0	13	3000
SN 2017eaw	2.7	15	300	(5)	2.2	7	2600
Mean	⋯	⋯	⋯	⋯	1.92	13.0	3320
Std. dev.	⋯	⋯	⋯	⋯	0.88	4.7	508

Note. References. (1) (R. Ouchi & K. Maeda 2021); (2) (M. C. Bersten et al. 2011); (3) (L. Tomasella et al. 2013); (4) (M. Dall'Ora et al. 2014); (5) (S. D. Van Dyk et al. 2019).

is somewhat larger. Despite this difference, both events are characterized by unusually large progenitor radii. To evaluate the sensitivity of the inferred parameters to the choice of reference object, we additionally applied the same scaling relations using several well-studied Type IIP SNe whose physical properties have been independently constrained through progenitor detections and/or hydrodynamic and radiative-transfer modeling. The comparison sample consisted of SN 1999em (A. Elmhamdi et al. 2003; M. C. Bersten et al. 2011), SN 2012A (L. Tomasella et al. 2013), SN 2012aw (S. Bose et al. 2013; M. Dall'Ora et al. 2014), and SN 2017eaw (S. D. Van Dyk et al. 2019) (see Table 3). Applying the scaling relations to these objects yielded average physical parameters of $E_k = (1.9 \pm 0.9) \times 10^{51}$ erg, $M_{ej} = 13 \pm 4.5\,M_\odot$, and $R_0 = 3300 \pm 500\,R_\odot$ for SN 2023gfo. The remaining dispersion likely reflects both the diversity of the reference SNe and the simplifying assumptions inherent in the analytic scaling relations, which describe the explosion using a limited set of observables. In particular, the progenitor radius derived using SN 2009kf ($3500\,R_\odot$) is fully consistent with the range obtained from the independent comparison sample (2600–$3900\,R_\odot$), indicating that the inference of an extended progenitor is not driven solely by the choice of SN 2009kf as the reference object. The estimates obtained using SN 2009kf are therefore broadly consistent with those derived from other well-studied Type IIP SNe.

The comparison sample further suggests that the explosion energy of SN 2023gfo is somewhat larger than, but still comparable to, those of ordinary Type IIP SNe. In contrast, the progenitor radius remains systematically larger than those of typical red supergiants regardless of the adopted reference object. Therefore, the inference of an unusually extended progenitor appears to be a robust result of the scaling analysis. SN 2009kf shares several observational and inferred physical properties with SN 2023gfo, suggesting that the two SNe may have experienced a similar evolutionary process prior to explosion. R. Ouchi & K. Maeda (2021) interpreted the extremely large progenitor radius of SN 2009kf as evidence for an expanded envelope produced by intense pre-SN energy injection (R. Ouchi & K. Maeda 2019). Although this interpretation is not unique, SN 2023gfo may likewise have undergone substantial pre-SN energy injection that significantly expanded its envelope before core collapse. Although the exact physical mechanism responsible for such energy deposition remains uncertain, one possibility is energy transport by convectively excited waves generated during the final nuclear-burning stages prior to core collapse (J. Fuller 2017).

Another possibility to explain the anomalous observational properties of SN 2023gfo is the ejecta–CSM interaction. Our first spectrum was obtained at $t = 4$ days. For some SNe IIP, the very early-phase spectrum often shows highly ionized emission lines, such as the Balmer series, as an interaction feature. However, our spectrum just shows a blue continuum. At $t = 11$ days, broad absorption lines from the ejecta component were found. This fact contradicts the interpretation of an interaction-powered SN. For interaction-powered Type IIP/IIL SNe, the spectra do not show absorption lines because the continuum is diluted by the interaction (N. N. Chugai 2001).

As another key observational evidence of CSM interaction, a rapid rise and bumpy structures are expected in the bluer-band light curves (T. J. Moriya & A. Singh 2024). Such features were not seen in SN 2023gfo. Color evolution is consistent with that of other normal SNe IIP during the plateau phase (see Figure 3). Therefore, we conclude that there is no indication of ejecta–CSM interaction in our observations.

5. Conclusion

In the present work, we presented multiband optical and NIR light curves (see Tables 4, 5, and 6) and optical spectra of SN 2023gfo. From the observed light curves, bolometric luminosity, and spectral data, we derived the plateau luminosity and duration, as well as the expansion velocity. SN 2023gfo is characterized by a high peak luminosity of $(5.9 \pm 1.5) \times 10^{42}$ erg s^{-1}, a high expansion velocity of 13,800 km s^{-1}, and a normal plateau duration of approximately 108 days.

We applied these observational parameters to analytical scaling relations based on D. V. Popov (1993) to estimate the physical properties of the explosion and progenitor. The results indicate an explosion energy consistent with those of typical Type IIP SNe, a slightly lower ejecta mass, and a significantly enlarged progenitor radius.

Such a combination of parameters is qualitatively consistent with scenarios involving pre-SN energy injection into the stellar envelope, which can lead to substantial radial inflation. A similar interpretation has been proposed for the peculiar Type IIP SN 2009kf (R. Ouchi & K. Maeda 2021). In this context, SN 2023gfo may represent another example of a Type IIP SN associated with an unusually extended progenitor.

Table 4
Optical Photometry of SN 2023gfo Obtained with the GIT

JD − 2400000	*g* (mag)	*r* (mag)	*i* (mag)	*z* (mag)
60056.37	⋯	⋯	⋯	15.327 ± 0.063
60063.32	15.949 ± 0.026	15.280 ± 0.035	15.014 ±0.045	14.894±0.047
60064.35	15.881 ± 0.026	15.008 ± 0.032	⋯	⋯
60082.25	16.283 ± 0.044	15.288 ± 0.046	14.990 ± 0.053	14.817 ± 0.050
60086.26	16.312 ± 0.021	15.299 ± 0.030	15.019 ± 0.039	14.772 ± 0.074
60091.26	17.347 ± 0.278	15.373 ± 0.087	15.023 ± 0.040	⋯
60092.21	16.456 ± 0.055	15.423 ± 0.058	15.104 ± 0.091	14.855 ± 0.129
60099.23	16.572 ± 0.063	15.306 ± 0.039	14.932 ± 0.042	14.866 ± 0.058
60102.25	16.731 ± 0.026	15.501 ± 0.030	⋯	⋯
60109.22	16.765 ± 0.054	15.255 ± 0.033	15.201 ± 0.130	⋯

Note. Magnitudes are reported in the AB system and have not been corrected for host-galaxy reddening. Unavailable measurements are indicated by ⋯.

Table 5
BVRI Photometry of SN 2023gfo Obtained with HOWPol

MJD	*B*	*V*	*R*	*I*
60055.78087	16.433 ± 0.007	15.707 ± 0.017	15.015 ± 0.000	14.775 ± 0.001
60056.72727	16.406 ± 0.004	15.620 ± 0.001	15.120 ± 0.002	14.705 ± 0.001
60060.66319	16.444 ± 0.016	15.547 ± 0.005	⋯	14.607 ± 0.001
60073.58303	16.612 ± 0.003	15.584 ± 0.001	14.885 ± 0.001	14.428 ± 0.001
60079.64774	16.832 ± 0.005	15.619 ± 0.001	14.869 ± 0.000	14.421 ± 0.003
60111.00000	17.990 ± 0.046	16.181 ± 0.007	15.289 ± 0.002	14.719 ± 0.002

Note. All magnitudes are reported in the Vega system and have not been corrected for host-galaxy reddening. Unavailable measurements are indicated by ⋯.

Table 6
Near-infrared Photometry of SN 2023gfo Obtained with kSIRIUS

MJD	*J* (mag)	*H* (mag)	*K* (mag)
60056.7	14.038 ± 0.011	13.749 ± 0.020	13.659 ± 0.035
60060.6	13.954 ± 0.010	13.655 ± 0.020	13.394 ± 0.021
60065.6	13.809 ± 0.010	13.245 ± 0.025	13.148 ± 0.013
60066.6	13.781 ± 0.009	13.440 ± 0.015	13.168 ± 0.017
60073.6	13.582 ± 0.025	13.363 ± 0.046	13.042 ± 0.159
60079.6	13.617 ± 0.011	13.126 ± 0.028	12.971 ± 0.021
60098.6	13.634 ± 0.010	13.134 ± 0.021	12.979 ± 0.015
60151.5	14.279 ± 0.025	13.878 ± 0.039	13.510 ± 0.063
60154.5	14.377 ± 0.023	14.066 ± 0.029	13.865 ± 0.040
60304.8	16.934 ± 0.075	⋯	⋯
60305.9	17.044 ± 0.095	16.162 ± 0.065	15.804 ± 0.064
60316.8	17.012 ± 0.068	16.531 ± 0.080	15.966 ± 0.070
60337.9	17.143 ± 0.093	16.575 ± 0.099	16.111 ± 0.106

Note. All magnitudes are reported in the Vega system and have not been corrected for host-galaxy reddening. Unavailable measurements are indicated by ⋯.

This scenario can potentially explain the large progenitor radius and high luminosity derived from the observational properties of SN 2023gfo. Alternatively, the ejecta–CSM interaction scenario may also explain the observational features, although there is no clear observational evidence for such an interaction. Future theoretical studies should explore how pre-SN energy injection modifies the progenitor structure and whether the resulting envelope inflation can reproduce the high luminosity, normal plateau duration, and high expansion velocity observed in SN 2023gfo. Such models would provide testable predictions for light-curve and spectral evolution that could distinguish between inflated-envelope progenitors and alternative scenarios involving ejecta–CSM interaction.

Acknowledgments

We are grateful to graduate and undergraduate students for performing the NIR observations. This work was supported by Grant-in-Aid for Scientific Research (C) 22K03676. The Kagoshima University 1 m telescope is a member of the Optical and Infrared Synergetic Telescopes for Education and Research (OISTER) program funded by the MEXT of Japan. D.K.S. acknowledges the support provided by DST-JSPS under grant number DST/INT/JSPS/P363/2022. This work was supported by JSPS Bilateral Program Number JPJSBP 120227709. The spectra taken by the Seimei telescope are obtained with the KASTOR (Kanata And Seimei Transient Observation Regime) campaign (23A-N-CT10, PI: K.M.). The Seimei telescope at the Okayama Observatory is jointly operated by Kyoto University and the National Astronomical Observatory of Japan (NAOJ), with assistance provided by the Optical and Infrared Synergetic Telescopes for Education and Research (OISTER) program. K.M. acknowledges support from the Japan Society for the Promotion of Science (JSPS) KAKENHI grant Nos. JP24KK0070 and JP24H01810. The GROWTH-India Telescope (GIT) is a 70 cm telescope with a $0.^{\circ}7$ field of view, set up by the Indian Institute of Astrophysics (IIA) and the Indian Institute of Technology Bombay (IITB) with funding from Indo-US Science and Technology Forum and the Science and Engineering Research Board, Department

of Science and Technology, Government of India. It is located at the Indian Astronomical Observatory (IAO, Hanle). We acknowledge funding by the IITB alumni batch of 1994, which partially supports the operation of the telescope. Telescope technical details are available at GROWTH-India website https://sites.google.com/view/growthindia/.

ORCID iDs

Masayuki Yamanaka https://orcid.org/0000-0001-9456-3709
Keiichi Maeda https://orcid.org/0000-0003-2611-7269
Avinash Singh https://orcid.org/0000-0003-2091-622X
Kenta Taguchi https://orcid.org/0000-0002-8482-8993
Miho Kawabata https://orcid.org/0000-0002-4540-4928
Koji S. Kawabata https://orcid.org/0000-0001-6099-9539
Devendra Sahu https://orcid.org/0000-0002-6688-0800
G. C. Anupama https://orcid.org/0000-0003-3533-7183

References

Anderson, J. P., Covarrubias, R. A., James, P. A., Hamuy, M., & Habergham, S. M. 2010, MNRAS, 407, 2660
Anderson, J. P., González-Gaitán, S., Hamuy, M., et al. 2014, ApJ, 786, 67
Barbarino, C., Dall'Ora, M., Botticella, M. T., et al. 2015, MNRAS, 448, 2312
Bersten, M. C., Benvenuto, O., & Hamuy, M. 2011, ApJ, 729, 61
Bose, S., Kumar, B., Sutaria, F., et al. 2013, MNRAS, 433, 1871
Botticella, M. T., Trundle, C., Pastorello, A., et al. 2010, ApJL, 717, L52
Cardelli, J. A., Clayton, G. C., & Mathis, J. S. 1989, ApJ, 345, 245
Chugai, N. N. 2001, MNRAS, 326, 1448
Dall'Ora, M., Botticella, M. T., Pumo, M. L., et al. 2014, ApJ, 787, 139
de Jaeger, T., Anderson, J. P., Galbany, L., et al. 2018, MNRAS, 476, 4592
Elmhamdi, A., Danziger, I. J., Chugai, N., et al. 2003, MNRAS, 338, 939
Ertini, K., Anderson, J. P., Folatelli, G., et al. 2026, arXiv:2602.03638
Filippenko, A. V. 1997, ARA&A, 35, 309
Flewelling, H. A., Magnier, E. A., Chambers, K. C., et al. 2020, ApJS, 251, 7
Fukugita, M., Ichikawa, T., Gunn, J. E., et al. 1996, AJ, 111, 1748
Fuller, J. 2017, MNRAS, 470, 1642
Fulton, M., Srivastav, S., Nicholl, M., et al. 2023, Transient Name Server Classification Report 2023-871, 1,
Hamuy, M. 2003, ApJ, 582, 905
Heger, A., Fryer, C. L., Woosley, S. E., Langer, N., & Hartmann, D. H. 2003, ApJ, 591, 288
Huang, F., Wang, X., Zhang, J., et al. 2015, ApJ, 807, 59
Inserra, C., Turatto, M., Pastorello, A., et al. 2011, MNRAS, 417, 261
Karachentsev, I. D., & Nasonova, O. G. 2013, MNRAS, 429, 2677
Kasen, D., & Woosley, S. E. 2009, ApJ, 703, 2205
Kawabata, K. S., Nagae, O., Chiyonobu, S., et al. 2008, SPIE, 7014, 70144L
Khazov, D., Yaron, O., Gal-Yam, A., et al. 2016, ApJ, 818, 3
Krisciunas, K., Hamuy, M., Suntzeff, N. B., et al. 2009, AJ, 137, 34
Kumar, R., Salgundi, A., Swain, V., et al. 2023, GCN, 35041, 1
Kurita, M., Kino, M., Iwamuro, F., et al. 2020, PASJ, 72, 48
Li, W., Leaman, J., Chornock, R., et al. 2011, MNRAS, 412, 1441
Maguire, K., Di Carlo, E., Smartt, S. J., et al. 2010, MNRAS, 404, 981
Martinez, L., Bersten, M. C., Anderson, J. P., et al. 2022, A&A, 660, A41
Matsubayashi, K., Tsutsui, H., Nakaya, H., et al. 2025, PASJ, 77, 1065
Minkowski, R. 1941, PASP, 53, 224
Moriya, T. J., & Singh, A. 2024, PASJ, 76, 1050
Nagayama, T., & Nakaya, H. 2024, SPIE, 13096, 130963I
Osterbrock, D. E., & Ferland, G. J. 2006, Astrophysics of Gaseous Nebulae and Active Galactic Nuclei (Univ. Science Books)
Ouchi, R., & Maeda, K. 2019, ApJ, 877, 92
Ouchi, R., & Maeda, K. 2021, MNRAS, 500, 1889
Pastorello, A., Valenti, S., Zampieri, L., et al. 2009, MNRAS, 394, 2266
Pettini, M., & Pagel, B. E. J. 2004, MNRAS, 348, L59
Popov, D. V. 1993, ApJ, 414, 712
Poznanski, D., Prochaska, J. X., & Bloom, J. S. 2012, MNRAS, 426, 1465
Roy, R., Kumar, B., Benetti, S., et al. 2011, ApJ, 736, 76
Sahu, D. K., Anupama, G. C., Srividya, S., & Muneer, S. 2006, MNRAS, 372, 1315
Singh, A., Teja, R. S., Moriya, T. J., et al. 2024, ApJ, 975, 132
Skrutskie, M. F., Cutri, R. M., Stiening, R., et al. 2006, AJ, 131, 1163
Smith, K. W., Smartt, S. J., Young, D. R., et al. 2020, PASP, 132, 085002
Sorce, J. G., Tully, R. B., Courtois, H. M., et al. 2014, MNRAS, 444, 527
Springob, C. M., Masters, K. L., Haynes, M. P., Giovanelli, R., & Marinoni, C. 2009, ApJS, 182, 474
Stetson, P. B. 1987, PASP, 99, 191
Tody, D. 1986, SPIE, 627, 733
Tody, D. 1993, ASPC, 52, 173
Tomasella, L., Cappellaro, E., Fraser, M., et al. 2013, MNRAS, 434, 1636
Tonry, J., Denneau, L., Weiland, H., et al. 2023, Transient Name Server Discovery Report 2023-858, 1,
Tonry, J. L., Denneau, L., Heinze, A. N., et al. 2018, PASP, 130, 064505
Tully, R. B., Courtois, H. M., Dolphin, A. E., et al. 2013, AJ, 146, 86
Tully, R. B., Courtois, H. M., & Sorce, J. G. 2016, AJ, 152, 50
Valenti, S., Sand, D., Pastorello, A., et al. 2014, MNRAS, 438, L101
Van Dyk, S. D., Zheng, W., Maund, J. R., et al. 2019, ApJ, 875, 136
Yamanaka, M., Fujii, M., & Nagayama, T. 2023, PASJ, 75, L27
Yang, Y., Brink, T. G., Zheng, W., et al. 2023, Classification and extinction estimate for SN 2023gfo, TNS Astronote 2023-95,
Yaron, O., Perley, D. A., Gal-Yam, A., et al. 2017, NatPh, 13, 510